

# **Lawrence Berkeley National Laboratory**

## Lawrence Berkeley National Laboratory

**Title**

Energy Amplification and Beam Bunching in a Pulse Line Ion Accelerator

**Permalink**

<https://escholarship.org/uc/item/20z5t7rr>

**Authors**

Roy, Prabir K.  
Waldron, William L.  
Yu, Simon S.  
et al.

**Publication Date**

2006-03-26

Peer reviewed

# Energy Amplification and Beam Bunching in a Pulse Line Ion Accelerator

Prabir K. Roy,<sup>1</sup> William L. Waldron,<sup>1</sup> Simon S. Yu,<sup>1</sup> Joshua E. Coleman,<sup>1</sup> Enrique Henestroza,<sup>1</sup> David P. Grote,<sup>2</sup> David Baca,<sup>1</sup> Frank M. Bieniosek,<sup>1</sup> Richard J. Briggs,<sup>3</sup> Ronald C. Davidson,<sup>4</sup> Shmuel Eylon,<sup>1</sup> Alex Friedman,<sup>2</sup> Wayne G. Greenway,<sup>1</sup> Matthaeus Leitner,<sup>1</sup> Grant B. Logan,<sup>1</sup> Louis L. Reginato,<sup>1</sup> and Peter A. Seidl<sup>1</sup>

<sup>1</sup>*Lawrence Berkeley National Laboratory, Berkeley, CA 94720, USA*  
<sup>2</sup>*Lawrence Livermore National Laboratory, Livermore, CA 94550, USA*

<sup>3</sup>*SAIC, Alamo, CA 94507, USA* and

<sup>4</sup>*Princeton Plasma Physics Laboratory, New Jersey 08543, USA*

In a first beam dynamics validation experiment for a new Pulse Line Ion Acceleration (PLIA) concept, the predicted energy amplification and beam bunching were experimentally observed. Beam energy modulation of -80 keV to +150 keV was measured using a PLIA input voltage waveform of -21 kV to +12 kV. Ion pulses accelerated by 150 keV, and bunching by a factor of 4 were simultaneously achieved. The measured longitudinal phase space and current waveform of the accelerated beam are in good agreement with 3-D particle-in-cell simulations.

PACS numbers: 52.59.Bi, 29.27.Ac, 41.85.p, 29.27.a, 41.75.Ak, Cn, 41.85Ct

Intense ion pulses of moderate energy offer an attractive driver for heating dense matter uniformly to extreme conditions, because their energy deposition is nearly classical and shock-free. Simultaneous transverse and longitudinal beam compression, along with rapid beam acceleration, are being studied as a means of generating such beams, which will be used for warm dense matter (WDM) [1–3], high energy density physics, and fusion [4] studies. Recent experiments on radial [5–10] and longitudinal [11, 12] compression of neutralized intense beams demonstrated significant enhancements in beam intensity. The experiments are in quantitative agreement with theory and simulations [13–18]. In parallel with beam compression studies, a new method of accelerating these intense ion bunches was conceived [19] and studied using analytic theory and simulations [19–24]. The Pulse Line Ion Accelerator (PLIA) potentially offers cost-effective high-gradient ion beam acceleration at high line charge density. A PLIA can accelerate beams of any pulse length, in principle, but is best suited as an accelerator for intense bunches with pulse lengths of tens of centimeters. This parameter regime is not well matched to RF accelerators. The major advantage of the PLIA concept is its potential for a significant reduction in the cost per MeV compared to induction linacs, for example.

The PLIA is a helical coil structure, submersed in a dielectric medium (oil) and powered by a pulsed high voltage waveform to impart beam energy gains many times higher than the input voltage to the helix. Ions are accelerated in the helical structure by a traveling electric field given by

$$E_z = \frac{2V_0}{\Delta z} \simeq \frac{2V_0}{\tau_c v_c} = \frac{2V_0}{\tau_c (L_0 C_0)^{-1/2}}, \quad (1)$$

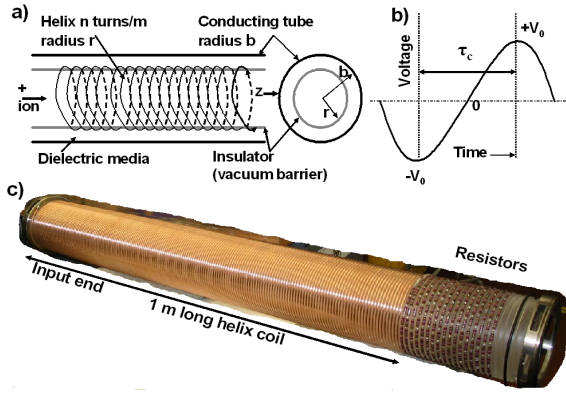
where  $2V_0$  is the incremental voltage change of a ramped pulse over an incremental distance  $\Delta z$ ,  $\tau_c$  is the duration of the ramped pulse, and  $v_c$ ,  $L_0$  and  $C_0$  are the circuit speed, the equivalent inductance, and the equivalent capacitance per unit length of the transmission line,

respectively. At the low frequencies involved, the wave propagates with almost no dispersion, so the wave pulse shape is preserved as it progresses downstream; that is, the voltage profile  $V(z - v_ct)$  changes only slightly with time. Figure 1(a) is a schematic representation of a helical pulse line structure.

Figure 1(b) is a simple applied voltage profile on the helix coil. Figure 1(c) shows the helical structure for this experiment, the parameters of which are listed in Table I. The input end of the helix is shorted to the outer conducting tube (ground). Transformer coupling from a loosely-coupled primary winding to the helix allows the input feedthrough voltage to be a fraction of the helix voltage. A primary strap with one or two turns, driven by a low-impedance pulsed-power source is placed a short distance radially outward from the grounded input end of the helix. A fraction of the flux created by the primary strap links to the helix, and this flux generates an axial voltage gradient along the input region of the helix. Downstream, the helix is terminated into its characteristic impedance via a string of resistors helically wound with a pitch similar to that of the helix. This serves to minimize reflections which could distort the voltage waveform. The low voltage test of pulse propagation on the helix shown in Fig. 2 verifies the propagation over 1m at a wave speed of 1.92 m/ $\mu$ s with minimal distortion.

The combination of pulse power drive with well-known helical slow wave structures is a unique feature of the PLIA. It is somewhat reminiscent of an earlier proposal to use a helix line to generate a moving magnetic well in the ERA [25].

The beam is approximately synchronous with the traveling wave and is continuously accelerated throughout the entire length,  $l$ , of the helical structure, leading to a final energy gain  $\Delta V \approx E_z l \gg 2V_0$ , where  $V_0$  is a nominal peak input voltage. Depending on the timing of the injected ion pulse, an additional acceleration up to  $V_0$  can occur in the transformer coupling region and/or the terminating resistor region. In addition to provid-



ing effective energy gain, the PLIA offers flexibility in manipulating the longitudinal phase space of the beam bunch. This is accomplished by appropriate shaping of the input voltage pulse and judicious timing of the pulse relative to the beam. This feature allows imparting a velocity ‘tilt’ to the beam to cause bunching and counter the longitudinal space-charge induced debunching [24].

TABLE I: Helix numerical parameters.

Parameter	Symbol	Unit	Value
Helix radius	$r$	cm	8.1
Ground return radius	$b$	cm	11.75
Helix pitch	$n$	turns/m	240
Effective helix length	$l$	m	1
Dielectric constant (oil)	$\epsilon$		2.3
Capacitance	$C_0$	pF/m	344
Inductance	$L_0$	$\mu\text{H}/\text{m}$	783
Impedance	$Z_0$	$\Omega$	1509
Wave velocity	$v_c$	m/s	$1.93 \times 10^6$

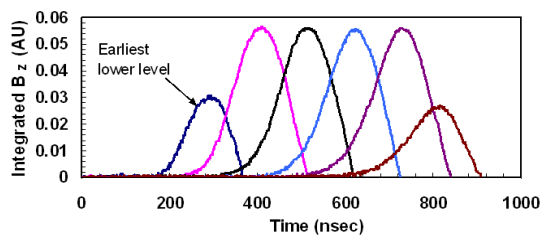


FIG. 2: Low voltage test of pulse propagation measured with a B-dot loop at 20.3 cm intervals. The earliest lower level signal is near the primary strap and the last signal is midway through the resistive termination string.

The helix with the parameters in Table I and a two-turn primary was installed on an ion beam line, as shown

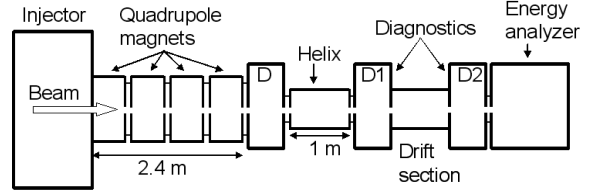


FIG. 3: Experimental configuration of the PLIA with a  $\text{K}^+$  beam injector, transport by 4 pulsed quadrupole magnets, 1 m long helix section, diagnostics, and an electrostatic energy analyzer.

in Fig. 3. The PLIA experiment used the same front end as the earlier Neutralized transverse focusing [5–10] and Neutralized longitudinal focusing [11, 12]. It consisted of a 350 keV,  $\approx 36$  mA  $\text{K}^+$  beam from an alumino-silicate source powered by a Marx generator, with variable pulse length from 300 ns to 20  $\mu\text{sec}$ . Four pulsed quadrupole magnets were used to control the beam envelope. The beam was apertured to  $\approx 1$  mA upstream of the PLIA section. Two removable diagnostics, separated by one meter, were located downstream of the helix section to measure the beam current profile, and followed by an electrostatic energy analyzer (EEA) to measure the longitudinal phase space. The energy analyzer used a 90-degree cylindrical first-order focus with a bend radius of 0.5 m; bipolar deflection plate voltages up to  $\pm 50$  kV were used to measure singly-ionized particles up to 1 MeV.

Before powering the helix section, the head-to-tail energy profile of the 350 keV, long-pulse (19  $\mu\text{s}$ ) beam was measured using the EEA as shown in Figure 4(a). This was done by varying the DC voltage of the electrostatic dipole, and collecting the beam current at the exit of the EEA with a Faraday cup. The Marx voltage waveform is shown in Figure 4(b). Except for beam dynamics effects introduced by time-of-flight and beam aperturing, the Marx waveform and the EEA energy profile were similar. The energy distribution provided by the EEA agreed with the capacitive monitor of the Marx voltage to about 2%.

A voltage pulser was applied to the input end of the PLIA. The pulser was a charged capacitor bank which was switched to the low-impedance helix primary through a triggered spark gap. Figure 5 shows the bipolar helix voltage waveform used for these initial tests of PLIA beam dynamics. The PLIA exhibited puzzling flashovers at relatively low voltages. For these experiments, the voltage swing was limited to 33 kV, in order to maintain shot-to-shot reproducibility. This corresponds to an average ion acceleration gradient of  $\approx 150$  kV/meter. Even at that voltage, a flashover was observed (light emission) on the interior of the helix beam tube, but the waveforms at the exit were reproducible. The problem continues to be investigated, including plans to test a PLIA with the insulating beam tube interrupted with voltage grading conductors.

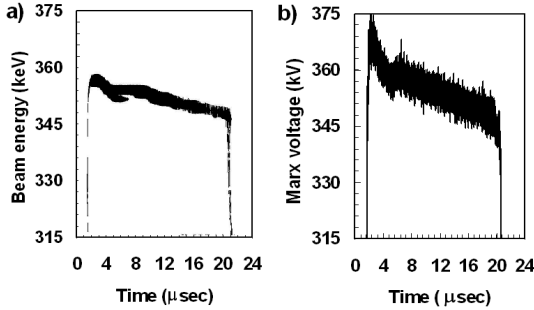


FIG. 4: a) Longitudinal time-energy phase space as measured using the EEA with the helix unpowered; b) Marx voltage waveform.

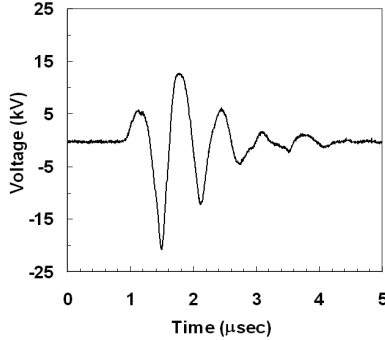


FIG. 5: Voltage waveform measured at the exit of the helix. The voltage and time interval associated with the first full peak-to-peak swing are 33 kV and 300 ns, respectively.

The helix voltage pulse was applied to the plateau portion of the beam, between 10 and 15  $\mu$ s after the beam head [see Fig. 4(a)], where the energy was nearly constant at the PLIA entrance. Figure 6(a) shows the measured longitudinal phase space of the beam after the helix voltage was applied. The initially flat energy profile then exhibited pronounced peaks and valleys. Note that the applied voltage waveform had about 5 oscillations of varying magnitudes. One expected that the portions of the beam riding on the positive slopes of the waveform were accelerated while the beam particles riding on the negative slopes decelerated. Indeed, the frequency in the longitudinal phase space coincided with that of the helix voltage waveform, and the 5 peaks and valleys of varying magnitudes in Fig. 6(a) could be identified with the positive and negative slopes of the voltage waveform. In these experiments, parts of the beam peaks reached as high as  $\sim 500$  keV and valleys as low as  $\sim 270$  keV. The beam energy change in this measurement ranged from -80 keV to +150 keV. Note that the helix voltage had a maximum range of -21 kV to +12 kV (Fig. 5).

The result of a WARP [26] particle-in-cell simulation is shown in Fig. 6(b), using an axisymmetric model with electrostatic beam self fields. The model results closely matched those of the experiment, when the beam was injected from the source using the Marx waveform taken from the experiment and transported through the entire

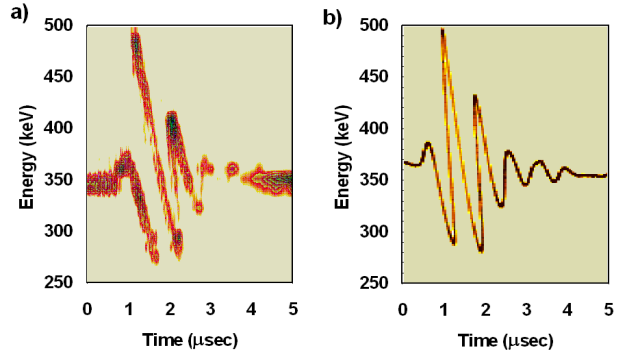


FIG. 6: a) Time-energy phase space of 350 keV beam after passing through the energized PLIA. With the input voltage waveform of Fig. 5, an energy modulation of -80 keV to +150 keV was measured; b) WARP3D simulation for similar conditions.

beamline. The conductor geometry from the experiment was included as a set of Dirichlet boundary conditions on the potential, and as a particle absorbing boundary. An idealized model of the helix was used whereby the helix waveform was advected along the surface of a conducting cylinder, at the circuit wave speed  $v = 2 \text{ m}/\mu\text{s}$ . The waveform from the experiment was used to specify the voltage as a function of time at the start of the helix, as shown in Fig. 5 and time-shifted assuming dispersion-free propagation. At each simulation time step, this provided a spatial variation of the voltage along the helix wall used in the calculation of the electric potential. Space charge effects were included up to the entrance slit of the EEA, where the particle current was further reduced. The particles were then tracked ballistically (since the self fields were negligible) to the end of the EEA to produce the distribution in Fig. 6(b).

Figure 7(a) shows the beam current amplification factor (ratio of current with helix power on to current with power off) as a function of time, measured using a Faraday cup at the second diagnostic section (located immediately upstream of the energy analyzer). Multiple peaks were observed in the current profile, coinciding with the upward swings of the helix voltage pulse. Two of the peaks were double peaks, with sharp spikes at the start and end of the peak; this structure was due to particle overtaking (wave breaking) in the  $(z, v_z)$  phase space. The WARP simulation yields similar structures, as can be seen in Fig. 7(b). We have observed very similar structures in previous neutralized drift compression experiments [11, 12]. The higher amplitudes and the correspondingly closer double peaks in the simulations indicate that the idealized WARP model is predicting less particle overtaking than in the experiments. The structure and location of the current peaks from particle overtaking are very sensitive to the details of the helix waveform propagation and diagnostics location. The same feature can be seen in the longitudinal phase-space comparison of Fig. 6. The simulation of Fig. 6(b) show

steeper slopes in the energy swings, compared to the experiment Fig. 6(a), where the extent of particle overtaking is somewhat greater.

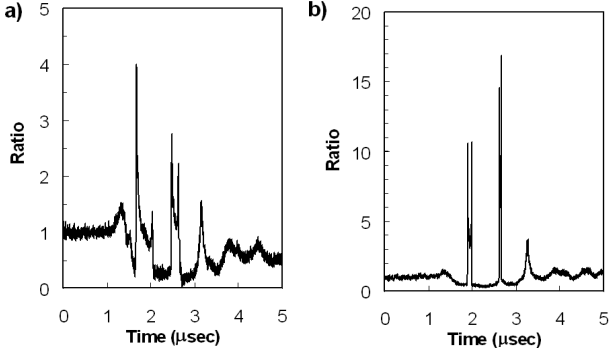


FIG. 7: Beam current amplification factor, (a) as measured using a Faraday cup upstream of the energy analyzer; and (b) as simulated using the WARP code. The Faraday cup had a finite aperture as well as time resolution and was unable to measure the full beam bunch current variations predicted by the simulation.

Finally, as an example of how the PLIA can accelerate whole bunches, a short pulse was accelerated. To perform this experiment, the Marx voltage pulse was shortened to 350 ns (FWHM) [see Fig. 8(a)], which was comparable to the beam transit time through the injector diode. The beam dynamics in the diode was entirely different from the Child-Langmuir flow characteristic of the long pulse. These transient effects led to a short pulse with a large energy tilt from head to tail [Fig. 8 (b)]. When the helix voltage pulse was applied by synchronizing the short pulse to the rising portion of the helix voltage waveform, the entire beam bunch was accelerated. The resulting longitudinal phase space is shown in Fig. 8(c). Note that the energy tilt of the beam bunch was also increased. This illustrates the potential flexibility in manipulating the longitudinal phase space by varying the input voltage wave shape and by varying the timing of the beam relative to the voltage waveform. This feature is of

great value in controlling the longitudinal space-charge debunching effects of an intense short pulse, as well as in providing the necessary velocity tilt for neutralized drift

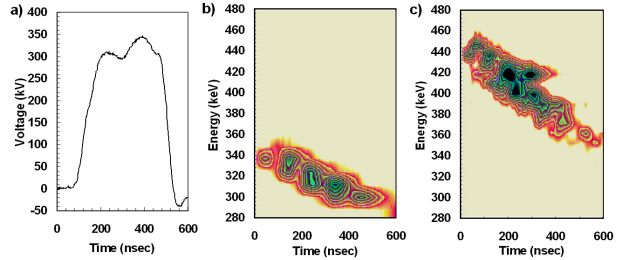


FIG. 8: Short-beam experiment on PLIA: (a) Marx voltage waveform; (b) beam time-energy phase space without helix power; and (c) phase space with helix powered.

compression.

In summary, the acceleration of non-relativistic  $K^+$  ion bunches with a helical slow wave structure submersed in a dielectric has been demonstrated. Due to the traveling wave providing the accelerating field, significant energy amplification has been achieved with modest voltage pulses. Vacuum flashover, which presently limits the acceleration gradient to  $\leq 150$  kV/m is being investigated. When solved, the PLIA concept has the potential to achieve high acceleration gradients at a modest cost. We are performing end-to-end simulations of drivers for WDM experiments, utilizing PLIA modules followed by final neutralized drift compression and focusing.

This research was performed under the auspices of the U.S. Department of Energy by the University of California Lawrence Livermore and Lawrence Berkeley National Laboratories and the Princeton Plasma Physics Laboratory, under Contract Nos. W-7405-Eng-48, DE-AC02-05CH11231, and DE-AC02-76CH03073. We thank Dr. J. Barnard, Dr. C. Celata, Dr. E. Lee, Dr. A. Molvik, Dr. W. M. Sharp and Dr. D. R. Welch for useful discussions.

- 
- [1] P. Renaudin et al., Phys. Rev. Lett. **91**, 075002 (2003).  
[2] A. Kozyreva et al., Phys. Rev. E **68**, 056406 (2003).  
[3] J. J. Barnard et al., in *Proc. of the 2005 Particle Accelerator Conf.*, edited by C. Horak, (IEEE, 2005), p. 2568.  
[4] W. M. Sharp et al., Nucl. Instrum. Meth. Phys. Res. A **544**, 398 (2005).  
[5] S. S. Yu et al., in *Proc. of the 2003 Particle Accelerator Conf.*, edited by J. Chew, (IEEE, 2003), p. 98.  
[6] E. Henestroza, et al., Phys. Rev. ST Accel. Beams **7**, 083501 (2004).  
[7] P. K. Roy et al., Phys. of Plasmas **11**, 2890 (2004).  
[8] B. G. Logan et al., Nucl. Fusion **45**, 131 (2005).  
[9] C. Thoma et al., Phys. of Plasmas **12**, 043102 (2005).  
[10] P. K. Roy et al., Nucl. Instrum. Meth. Phys. Res. A **544**, 225 (2005).  
[11] P. K. Roy et al., Phys. Rev. Lett. **95**, 234801 (2005).  
[12] C. Thoma et al., in *Proc. of the 2005 Particle Accelerator Conf.*, edited by C. Horak (IEEE, 2005), p. 4006.  
[13] D. D.-M. Ho et al., Particle Accelerators **35**, 15 (1991).  
[14] T. Kikuchi et al., Phys. of Plasmas **9**, 3476 (2002).  
[15] M. J. L. de Hoon et al., Phys. of Plasmas **10**, 855 (2003).  
[16] H. Qin et al., Phys. Rev. ST Accel. Beams **7**, 104201 (2004).  
[17] R. C. Davidson et al., Phys. Rev. ST Accel. Beams **8**, 064201 (2005).  
[18] D. R. Welch et al., Nucl. Instrum. Meth. Phys. Res. A **544**, 236 (2005).  
[19] R. J. Briggs et al., in *Proc. of the 2005 Particle Acceler-*

- ator Conf., edited by C. Horak (IEEE, 2005), p.440.
- [20] A. Friedman et al., *ibid.* (IEEE, 2005), p.339.
- [21] G. Caporaso el al., *ibid.* (IEEE, 2005), p.2330.
- [22] S.D.Nelson et al., *ibid.* (IEEE, 2005), p.2485.
- [23] W. L. Waldron et al., *ibid.* (IEEE, 2005), p.2092.
- [24] E. Henestroza et al., *ibid.* (IEEE, 2005), p.2032.
- [25] L. J. Laslett et al., in *Proc. of the 1969 Particle Accelerator Conf.*, edited by F. T. Howard (IEEE, 1969), p.1034.
- [26] D. P. Grote et al., in *AIP Conf. Proc.*, **749**, 55 (2005).